DYNAMIC RESPONSE PREDICTION OF THIN-WALLED WORKPIECE FIXTURE MILLING SYSTEM BASED ON PIEZOELECTRIC VIBRATION ENERGY COLLECTION STRUCTURE

Yunlei Wang[1], Shuang Deng[1], Dong Li[2], Huiyuan Guo[3], Junjin Ma[3]
[1]China Airborne Missile Academy, 471000, Luoyang, China
[2]Representative Office of Lu Zhuang stationed in a certain area of Xi'an, 710000, Xi'an, China
[3]School of Mechanical and Power Engineering, Henan Polytechnic University, 454003, Jiaozuo, China
Email: majhpu@hpu.edu.cn

Abstract - Thin-walled components are widely used in aerospace and other high-performance equipment due to their lightweight requirements, yet their complex geometries, thin walls, and low rigidity make them prone to machining-induced vibrations, particularly during milling. The significant time-varying dynamics caused by material removal and high cutting forces often lead to chatter, severely compromising machining quality and efficiency. To mitigate these vibrations, this study proposes an adjustable-stiffness and damping piezoelectric support structure designed to reinforce weak stiffness zones in thin-walled workpieces. First, a piezoelectric energy-harvesting support structure was optimized for vibration energy collection. Next, a workpiece-fixture configuration incorporating this piezoelectric support was developed. A dynamic response prediction model for the piezoelectric-enhanced workpiece-fixture system was then established and solved. Experimental validation demonstrated that the proposed system significantly reduces vibration amplitudes, confirming the effectiveness of both the piezoelectric energy-harvesting structure and the dynamic model.

Keywords: Thin-walled components, Milling processes, Machining vibration control, Piezoelectric vibration energy-harvesting fixtures, Dynamic modelling.

1. Introduction

The rapid advancement of aerospace industries has driven increasing demand for high-performance components, particularly thin-walled parts such as aero-engine blades and blisks. These components, characterized by complex geometries, thin walls, and low rigidity, exhibit pronounced time-varying dynamic behaviors during milling due to substantial material removal and fluctuating cutting forces. Such dynamics often trigger severe machining vibrations and deformations, compromising both surface quality and productivity. Effective vibration suppression is thus critical to enhancing the performance of thin-walled parts in aerospace applications.

Extensive research has been conducted globally to address vibration control in thin-walled component machining, yielding significant advancements. Current strategies primarily focus on vibration isolators, absorbers, and energy harvesters. For isolators, vibration suppression is typically achieved by optimizing machining parameters alongside isolation schemes. The foundational isolator, invented by Frahm in 1911 [1], functions by transferring vibrational energy from the primary structure to the isolator. Subsequent studies by Den et al. [2] detailed passive isolator design principles, while Zilletti et al. [3] explored optimization methods. Optimal isolator performance requires precise matching of the isolator's natural frequency with the excitation frequency. Although viscous dampers can broaden the operational frequency range, they often compromise peak damping performance. This limitation has spurred the development of adaptive-frequency isolators [4,5], which adjust equivalent stiffness or mass to tune their natural frequency. Isolators are thus classified as passive [6], semi-active [7], or active [8, 9], all of which absorb external vibrational energy. A key research challenge lies in harvesting this energy without sacrificing isolation efficacy. For vibration absorbers, three categories exist: passive, semi-active, and active [10]. While these dissipate energy

https://doi.org/10.17683/ijomam/issue22.v2.5

to suppress vibrations, machining processes offer opportunities for energy recovery, sparking growing interest in vibration energy harvesting [11]. The core objective is converting mechanical energy into electricity, though challenges persist in enhancing conversion efficiency for broader applications [12]. Stable mechanical vibration frequencies are critical for effective energy harvesting [13]. However, the time-varying dynamic model of thin-walled part machining lead to frequency instability, limiting the effectiveness of current vibration control and energy harvesting methods. Recent efforts have explored nonlinear structures—such as bistable [14], tristable [15], and quasi-zero-stiffness [16] systems—integrated with absorbers. While these multi-stable and quasi-zero-stiffness structures excel in low-frequency scenarios, their low-static-high-dynamic characteristics render them less suitable for milling-induced vibrations.

Recently, Energy harvesters have gained prominence as power sources for self-powered sensors, offering a sustainable alternative to battery-dependent systems [17-19]. Since duToit's foundational work on the electromechanical coupling model of 1D piezoelectric cantilever energy harvesters [20], subsequent studies have expanded this approach [21, 22]. For instance, Ali et al. [23] employed piezoelectric stacks as dual-function vibration absorbers and energy harvesters, optimizing system parameters to achieve broadband energy collection via frequency ratio tuning. Similarly, Dipak et al. [24] demonstrated energy harvesting under random excitations within specific frequency bands. Alternative mechanisms include electromagnetic induction, as explored by Sapinski [25] and Cho [26] to power magnetorheological (MR) damper-based vibration control systems, and Fang et al. [27] pendulum-like triboelectric-electromagnetic hybrid system, which enhanced efficiency through signal amplification circuits for unidirectional vibration harvesting. Grigorios et al. [28] designed semi-active piezoelectric mass-tuned damper, which enabled multimodal control via shunt circuits, and Manzoni et al. [29] optimized and designed tunable mass damper for multi-modal frequency matching while maintaining energy harvesting efficacy. Most such systems prioritize damping optimization to handle harmonic or random excitations across fixed frequency ranges. However, machining processes introduce unique challenges: harmonic excitations, often exhibit stepwise time-varying frequencies. To address this, future designs must integrate frequency-tunable, semi-active dampers capable of adapting to transient machining dynamics without compromising energy harvesting performance.

Current vibration control methods in machining suffer from significant limitations, including inefficient energy dissipation through damping, suboptimal frequency matching in micro-scale energy harvesters, bulky designs, and inadequate reliability for industrial applications. To overcome these challenges, a piezoelectric-based energy harvesting system featuring variable cross-section structures is proposed and tailored to machining dynamics. Through optimized structural design, this approach maximizes vibration energy absorption efficiency. In this process, a dynamic response prediction model is developed for the integrated thin-walled workpiece-fixture system incorporating the piezoelectric energy harvester. The research methodology follows three key phases: (1) optimization of the piezoelectric support structure's design parameters, (2) determination of the workpiece-fixture configuration for optimal energy harvesting, and (3) formulation and experimental validation of the system's dynamic response model. Experimental results demonstrate the optimized fixture system effectively suppresses milling vibration by improving energy absorption efficiency, verifying the practical applicability of the system in precision machining.

2. Introduction Dynamic Response Prediction Model for Thin-Walled Workpiece-Fixture Systems with Piezoelectric Energy Harvesting Structures

2.1 Optimization Design of Piezoelectric Energy-Harvesting Support Structures

To maximize vibration transmission and energy absorption at the workpiece-piezoelectric interface, the proposed design integrates miniature bolts at the midsection of a variable-cross-section piezoelectric unit, complemented by cylindrical pins with rounded tips. This configuration minimizes contact area with the workpiece while ensuring structural support and efficient energy transfer. The finalized unit meets all requirements for vibration energy harvesting in machining applications, which is shown in Figure 1.

As shown in Figure 2, to achieve optimal fusion between the piezoelectric energy-harvesting unit and fixture, a support structure was designed with dual symmetric arms. This configuration addresses two critical constraints: (1) minimal footprint for flexible spatial arrangement, and (2) compensation for assembly-induced tensile / compressive stresses caused by machining tolerances. The piezoelectric unit is centrally mounted between adjustable support arms, enabling dynamic tuning through gap modulation. Four design variants were systematically evaluated to balance structural rigidity and vibrational energy transfer efficiency.

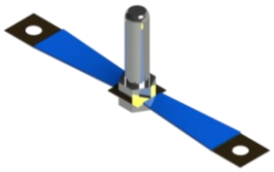

Figure 1: Piezoelectric vibration energy harvesting device

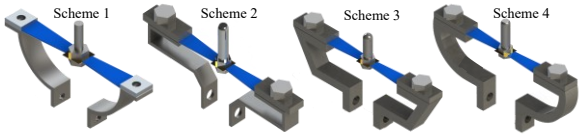

Figure 2: Double-support-arm structural device

All four aforementioned support arm configurations are capable of fulfilling the required functional objectives. Through simulation analyses and computational evaluations, configurations 2 and 3 are difficult to manufacture and inconvenient to clamp. In contrast, configurations 1 and 4 feature curved surface transitions, which not only facilitate easier machining and more convenient clamping but also confer superior stiffness and mitigate stress concentration effects. Furthermore, during the tensile deformation of the piezoelectric vibration energy harvesting unit, configuration 4 demonstrated enhanced stability compared to configuration 1, thereby better ensuring the flatness and stability of the piezoelectric patches. Consequently, configuration 4 was selected as the support structure for the piezoelectric vibration energy harvesting unit. To ensure a robust connection between the support structure of the piezoelectric vibration energy harvesting unit and the fixture body, a supporting frame structure was designed, as illustrated in Figure 3. For this frame, 304 stainless steel was adopted as the structural material.

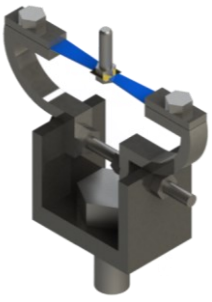

Figure 3: Piezoelectric Vibration Energy Harvesting Support Structure

To evaluate the vibration control effect of the aforementioned structure on thin-walled workpieces during support, it is necessary to establish a dynamic model of the workpiece-fixture system under the constraints of the piezoelectric vibration harvesting structure and solve its response. This work aims to provide a basis for realizing vibration control during the workpiece vibration process.

2.2 Configuration Determination of Piezoelectric Energy-Harvesting Support Fixtures for Thin-Walled Components

During the milling process of thin-walled components, piezoelectric support structures are applied to the regions of low stiffness in thin-walled workpieces to enhance their stiffness. However, when these piezoelectric support structures provide support to the thin-walled components, their layout within the fixture must be optimized. This optimization is intended to achieve effective vibration suppression by the piezoelectric support structures during the milling of thin-walled components.

In this study, the finite element software COMSOL was employed to perform simulation-based optimization of the fixture layout. For the definition of boundary conditions, fixed constraints were applied to both ends of the workpiece along its length, while an elastic base constraint was imposed on the middle section of the workpiece. This constraint configuration was designed to simulate the supporting effect of the piezoelectric support structures on the workpiece. Subsequent frequency-domain analysis was conducted to obtain the deformation contour of the thin-walled component. Specifically, the workflow was as follows: first, a three-dimensional (3D) model of the thin-walled workpiece was constructed. Second, material parameters and boundary conditions were assigned. Finally, the first-order natural frequency of the workpiece was calculated using a modal frequency solver, yielding a value of 163.87 Hz. The deviation between this simulated frequency and the theoretically computed first-order natural frequency was 2.67%. To facilitate excitation experiments using a standard shaker, the first-order natural frequency was adopted as the excitation frequency. An excitation force with an amplitude of 20 N was applied to the thin-walled component for frequency response analysis. The vibration displacement contour of the workpiece without support is presented in Figure 4.

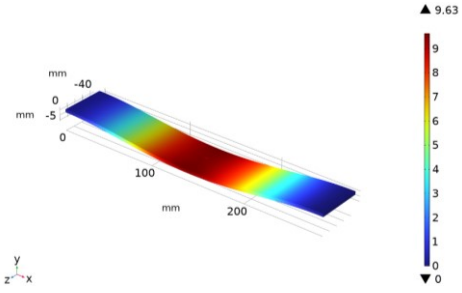

Figure 4: Vibration displacement contour of the workpiece under 20N excitation

As illustrated in Figure 4, the thin-walled workpiece exhibits excessive deformation under minimal Z-axis excitation (9.63 mm displacement), revealing its inherent structural compliance. The primary deformation zones localize near the mid-span along the X-axis (140 mm) and edges along the Y-axis (coordinates (140, 0) and (140, 45)), rendering the vibrational response unsuitable for precision machining. Given the symmetric distribution of maximal displacements, two piezoelectric support structures were strategically positioned at (140, 2.5) and (140, 42.5) to enhance stiffness while accommodating geometric constraints. Subsequent frequency-response analysis (Figure 5) demonstrates a 97% reduction in vibration amplitude (0.299 mm, 1/32 of the unsupported case), confirming the efficacy of targeted support placement. However, residual displacements suggest the need for additional damping structures to achieve stringent machining tolerances.

As evidenced by the displacement distribution in Figure 5, the workpiece's mid-span region remains structurally deficient. Persistent symmetry in vibrational response further necessitates additional damping measures. To address this, two supplementary supports were strategically integrated at coordinates (110, 22.5) and (170, 22.5), complementing the existing pair at (140, 2.5) and (140, 42.5). This configuration was adopted. Subsequent frequency-response analysis reveals a marked improvement in stiffness uniformity with the revised support topology effectively mitigating mid-span deformation while preserving structural equilibrium. As demonstrated in Figure 6, four support structures reduces the workpiece's vibrational displacement to 0.268 mm compared to the unsupported condition and a 10.4% improvement is obtained. At this point, increasing the number of additional support structures leads to a significant reduction in the effectiveness of suppressing workpiece vibration.

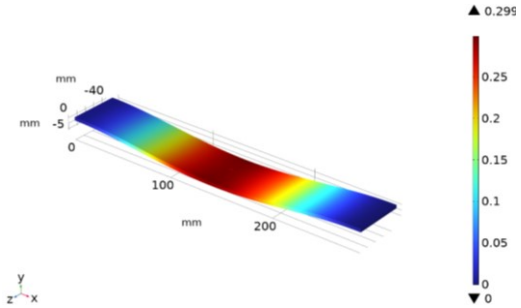

Figure 5: Vibration displacement contour of the workpiece under two supports

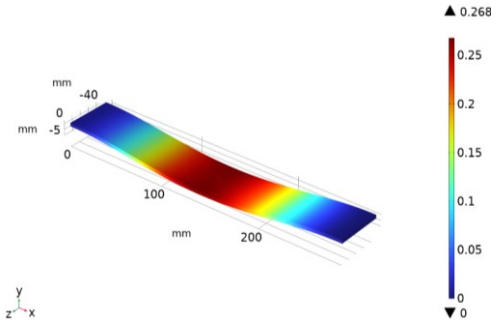

Figure 6: Vibration displacement contour of the workpiece under four supports

Under this circumstance, the four-support configuration achieved the expected vibration suppression. Meanwhile, the main vibration distribution of the structure is still concentrated in the middle dense part, and the four support structures arranged at four positions (140, 2.5), (140, 42.5), (110, 22.5) and (170, 22.5) are selected for application.

2.3 Dynamic Response Prediction of Thin-Walled Workpiece-Fixture System with Piezoelectric Energy Harvesting Structure

To achieve accurate performance evaluation of the thin-walled workpiece-fixture system based on the piezoelectric energy harvesting structure, it is necessary to establish the dynamic model of the workpiece-fixture system based on the piezoelectric energy harvesting structure.

During vibration, the guide rods connected with the piezoelectric energy harvesting fixture system will vibrate along with the workpiece vibration, which are played an important role on the workpiece-fixture system. Therefore, considering the mass of each structure's guide rod, the kinetic energy T_{sp} of the piezoelectric support fixture can be obtained as:

$$T_{sp} = \frac{1}{2}\sum_{i=1}^{b} m_{spi}\dot{w}^2\left(x_{si}, y_{si}, t\right) = \frac{1}{2}\sum_{i=1}^{b}\mathbf{q}\mathbf{M}_{\mathbf{spi}}\mathbf{q}^T \quad (1)$$

where m_{spi} is the mass of the i-th piezoelectric piezoelectric support structures, w is the displacement in the Z direction, $\mathbf{M_{spi}}$ denotes the mass matrix, $\mathbf{q}$ is the generalized velocity matrix.

Due to the fact that the stiffness of the guide rod, support arm, and support frame in the piezoelectric support structure is much higher than that of the variable-cross-section piezoelectric unit, when the piezoelectric vibration energy harvesting support structure is subjected to force due to workpiece vibration, the main deformation of the structure will occur on the variable-cross-section piezoelectric unit. And the deformation of the remaining parts will be much smaller than that of the variable-cross-

section piezoelectric unit, which can be ignored. Therefore, the elastic potential energy of the piezoelectric fixture can be expressed as:

$$\begin{aligned} U_{sp} &= \frac{1}{2}\sum_{i=1}^{a} k_{spi}\left(w\left(x_{si},y_{si},t\right)\right)^2 \\ &= \frac{1}{2}\sum_{i=1}^{a} k_{spi}\left(\sum_{i=1}^{n} q_n\left(t\right)W\left(x_{si},y_{si}\right)\right)^2 \\ &= \frac{1}{2}\sum_{i=1}^{a} \mathbf{q}\mathbf{K}_{\mathbf{spi}}\mathbf{q}^T \end{aligned} \tag{2}$$

where k_{spi} is the stiffness of the piezoelectric support structure, which can be calculated based on static analysis and is equal to 6112N/m, $\mathbf{K_{spi}}$ is the stiffness matrix.

Due to the piezoelectric effect of piezoelectric materials, electrical energy is excited during deformation, so it is necessary to determine the bending potential energy, which is expressed as

$$H_p = \frac{1}{2}\sum_{i=1}^{b}\sum_{j=1}^{2}\int_{V_p}\left(y^2 E_p \ddot{w}^2 + 2ye_{21}\vartheta_{21}\ddot{w} - \varepsilon^s \vartheta_{21}^2\right)dV_p \tag{3}$$

where i and j represent the i-th piezoelectric support structure and the j-th piezoelectric sheet, E_p is Young's modulus, e_{21} represents the piezoelectric constant, ε^s represents the dielectric constant, ϑ_{21} represents the electric field strength.

Thus, combining Eq.(1), Eq.(2) and Eq.(3), the modified Lagrangian equation of the workpiece-fixture system can be obtained and can be expressed by

$$\begin{aligned} &\frac{d}{dt}\left(\frac{\delta\left(T+T_{sp}\right)}{\delta\dot{\mathbf{q}}}\right) - \frac{\delta\left(T+T_{sp}\right)}{\delta\mathbf{q}} \\ &+ \frac{\delta\left(R+R_s\right)}{\delta\mathbf{q}} + \frac{\delta\left(U+U_{sp}+H_p\right)}{\delta\mathbf{q}} = \frac{\delta W}{\delta\mathbf{q}} \end{aligned} \tag{4}$$

To obtain the response of system, based on Eq.(4), the dynamic model of workpiece piezoelectric fixture dynamic system can be expressed as

$$\begin{cases} \mathbf{M}^*\ddot{\mathbf{q}}(t) + \mathbf{C}^*\dot{\mathbf{q}}(t) + \mathbf{K}^*\mathbf{q}(t) - \Theta\vartheta(t) = \mathbf{P}^*(t) \\ \frac{1}{2}C_p\ddot{\vartheta}(t) + \Theta q(t) + \frac{1}{R_L}\vartheta(t) = 0 \end{cases} \tag{5}$$

where **M***, **K*** and **C*** represent the modal mass, modal damping, and modal stiffness of the workpiece-fixture system respectively. R_L is the external circuit resistance, Θ is the electromechanical coupling coefficient, C_p is the capacitance of the piezoelectric vibration energy harvesting device, and its values along with other modified dynamic parameters are:

$$\begin{cases} \mathbf{M}^* = m\mathbf{M} + \sum_{i=1}^{b}\mathbf{M}_d \\ \mathbf{C}^* = \alpha m\mathbf{M} + \beta\mathbf{K} + \sum_{i=1}^{p} C_p \\ \mathbf{K}^* = D\mathbf{K} + \sum_{i=1}^{p}\mathbf{K}_{sp} \\ \mathbf{P}^* = \frac{F_z(t)\mathbf{W}^T}{m} \\ C_p = \frac{2\kappa_{uu}^s BL_1}{h_p} \end{cases} \tag{6}$$

For the convenience of calculation, an open circuit in the external circuit is considered, the external resistance R_L is positive infinity and the electrical energy generated by the bending of the piezoelectric sheet is 0. At this point, the voltage term in Eq.(4) and Eq.(5) can be ignored, and the dynamic model of the workpiece piezoelectric fixture becomes rewritten as

$$\mathbf{M}^*\ddot{\mathbf{q}}(t) + \mathbf{C}^*\dot{\mathbf{q}}(t) + \mathbf{K}^*\mathbf{q}(t) = \mathbf{P}^*(t) \tag{7}$$

To solve Eq.(4), performing Laplace transform on Eq. (4), in the Laplace domain, the dynamic model of the workpiece-fixture system is transformed into

$$\begin{aligned} &\left(s^2\mathbf{M}^* + s\mathbf{C}^* + \mathbf{K}^*\right)q\left(s\right) \\ &= \mathbf{P}\left(s\right) + \mathbf{M}^*\dot{q}_0 + \left(s\mathbf{M}^* + \mathbf{C}^*\right)q_0 \end{aligned} \tag{8}$$

To solve the Eq. (8), it is necessary to solve the characteristic problem of the corresponding undamped system. Therefore, the corresponding eigenvalue problem is

$$K^* c_i - \omega_{wsi}^2 M^* c_i = 0, i = 1,2,...,r \tag{9}$$

where ω_{wsi} represents the i-th modal frequency of the workpiece piezoelectric fixture, and $c_i = \begin{pmatrix} c_i^1 & c_i^r & \cdots & c_i^r \end{pmatrix}^T$ is the corresponding modal vector.

For the convenience of calculation, the natural frequency matrix Ω and modal vector matrix C are defined as follows:

$$\Omega = \begin{pmatrix} \omega_1 & & & \\ & \omega_2 & & \\ & & \ddots & \\ & & & \omega_r \end{pmatrix} \tag{10}$$

$$\mathbf{C}=\begin{pmatrix} c_1^1 & c_2^1 & \cdots & c_r^1 \\ c_1^2 & c_2^2 & \cdots & c_r^2 \\ \vdots & \vdots & \ddots & \vdots \\ c_1^r & c_2^r & \cdots & c_r^r \end{pmatrix} \tag{11}$$

Then, Eq. (10) and Eq. (11) satisfy the relationship $\mathbf{C}^T\mathbf{M}^*\mathbf{C}=\mathbf{I},\mathbf{C}^T\mathbf{K}^*\mathbf{C}=\mathbf{\Omega}^2$.

Next, by multiplying Eq. (8) by $\mathbf{C}^T$ on the left and $\boldsymbol{C}$ on the right, and based on the orthogonality of the modal vectors, the decoupled dynamic equation can be obtained by

$$\left(s^2\mathbf{I}+s\mathbf{C}'+\mathbf{\Omega}^2\right)q(s)=\mathbf{P}'(s) \tag{12}$$

where $\mathbf{P}'(s)=\mathbf{C}^T\left(\mathbf{P}(s)+\mathbf{M}^*\dot{q}_0+\left(s\mathbf{M}^*+\mathbf{C}^*\right)q_0\right)\mathbf{C}$, $\mathbf{C}'(s)=\mathbf{C}^TC^*\mathbf{C}$.

According to mathematical theory, the solution of equation Eq.(8) can be expressed as

$$s_i=-\zeta_i\omega_i\pm i\omega_i\sqrt{1-\zeta_i^2} \tag{13}$$

where $\zeta_i=\dfrac{1}{2\omega_i}\mathbf{C}'$.

Subsequently, the dynamic stiffness matrix $\mathbf{D}(s)$ of the second-order linear dynamic equation can be obtained by

$$\mathbf{D}(s)=s^2\mathbf{I}+s\mathbf{C}+\mathbf{\Omega}^2 \tag{14}$$

According to the residual theory, the transfer function $\mathbf{H}(s)$ of the thin-walled workpiece-the piezoelectric support fixture can be derived by

$$\mathbf{H}(s)=\left[\mathbf{D}(s)\right]^{-1}=\sum_{i=1}^{r}\frac{1}{s-s_i}\frac{x_ix_i^T}{x_i^T\dfrac{\partial D(s_i)}{\partial s_i}x_i} \tag{15}$$

Based on this, the dynamic response of the thin-walled workpiece-fixture systems with piezoelectric energy harvesting structures can be calculated by

$$\begin{aligned} q(t)&=L^{-1}\left[q(s)\right]=L^{-1}\left[\mathbf{H}(s)\mathbf{P}(s)\right] \\ &=\sum_{i=1}^{r}\frac{\left\{\int_0^t e^{s_i(t-\tau)}\left[x_i^T\mathbf{P}(\tau)+x_i^T\mathbf{C}(\tau)q_0\right]d\tau+e^{s_i(t-\tau)}\left[x_i^T\mathbf{M}q_0+s_ix_i^TCq_0\right]\right\}x_i}{x_i^T\dfrac{\partial\mathbf{D}(s_i)}{\partial s_i}x_i} \end{aligned} \tag{16}$$

Based on the relationship between the external load and the output voltage across the load resistor, the output voltage of the piezoelectric fixture in an open circuit state is obtained by

$$v(t)=e^{-\frac{h_pt}{2\kappa_{uu}^pBL_tR_L}}\int\left\{\begin{bmatrix}\int_{u=0}^{L_1}-e_{uv}E_ph_{ap}B\dfrac{\partial^3q(t)}{\partial x^2\partial t}du \\ +\int_{u=L_1+L_2}^{L}-e_{uv}E_ph_{ap}B\dfrac{\partial^3q(t)}{\partial x^2\partial t}du\end{bmatrix}e^{\frac{h_pt}{2\kappa_{uu}^pBL_tR_L}}\right\}dt+c \tag{17}$$

where c is a constant.

In milling of thin-walled workpieces, the initial displacement, initial velocity, and output voltage are all 0. After substituting the initial conditions and excitation into Eq.(16) and Eq.(17), the dynamic response and output voltage of the thin-walled workpiece piezoelectric fixture system under external excitation can be obtained.

3. Experimental Validation and Discussion

To validate the accuracy of the established model in solving structural vibration characteristics, vibration responses, and output voltages, a series of experiments were designed for verification. For this purpose, the workpiece-piezoelectric fixture system was first excited using a shaker, and the vibration responses of the workpiece were measured via accelerometers to verify the theoretical accuracy in solving vibration responses. Subsequently, machining tests were conducted to validate the vibration suppression effects on the vibration characteristics of both the workpiece-piezoelectric fixture system and the conventional workpiece-fixture system.

3.1 Dynamic Response Test of Workpiece-Fixture System

To validate the dynamic response of the workpiece-fixture system, a vibration test was conducted on the workpiece-piezoelectric fixture system using a shaker. During the test, three factors (excitation frequency, the number of piezoelectric support structures and resistance of the backend circuit) were considered to evaluate their effects on the vibration response. Based on initial test results, the modal frequency of the workpiece-fixture system was 166.321 Hz, so the excitation frequency test range was set to 150-300 Hz. Based on the fixture layout, 1, 2, and 4 piezoelectric support are selected for validation, respectively. Next, 10 kΩ, 20 kΩ, 30 kΩ, 40 kΩ, and 50 kΩ were selected as test parameters for verification. As shown in Figure 7, for the vibration response test of the workpiece, the fixture was fixed horizontally to facilitate the experiment, and the workpiece was excited transversely by the shaker. And the support layout of piezoelectric energy harvesting structures in fixture is observed in Figure 8(a). In addition, the external circuit used an adjustable resistor ranging from 0 to 100 kΩ to control the external circuit resistance, which is shown in Figure 8(b).

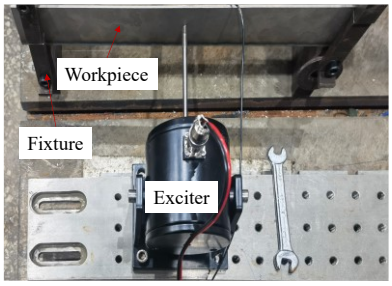

Figure 7: Exciter layout schematic diagram

Next, the workpiece-fixture system was tested using excitation at a fixed frequency of 200 Hz. Based on the vibration data, the workpiece's vibration acceleration was controlled at 0.3g, and at this state, the vibration amplitude was relatively large, enabling clear vibration feedback. Afterwards, with the same test platform parameters, sets of excitation tests were conducted on the workpiece-piezoelectric fixture system to verify the changes in vibration response. To verify the calculation results of the model, one group of data was selected for analysis. In order to compare the vibration suppression effect of the piezoelectric fixture, tests were carried out on the workpiece's vibration response under the workpiece without support, workpiece with one piezoelectric support (under different resistance values), workpiece with two piezoelectric supports (under different resistance values) and workpiece with four piezoelectric supports.

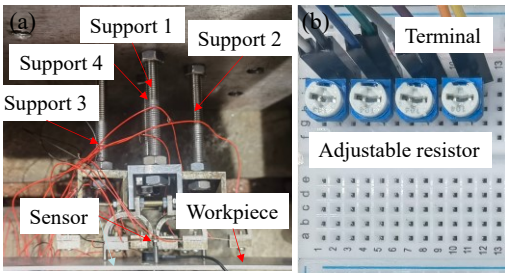

Figure 8: Workpiece fixture systems with different piezoelectric support and adjustable resistance circuits

To better demonstrate the vibration response of the workpiece-piezoelectric fixture system under different conditions, the vibration responses of the workpiece under different resistance parameters and piezoelectric supports are obtained, which are shown in Figure 9, Figure 10 and Figure 11. To facilitate a clearer observation of the vibration response, a 0.1-second data segment was selected for comparison.

Figure 9 illustrates the comparison of vibration responses with one piezoelectric support versus no piezoelectric support. Figure 9(a) shows the workpiece vibration displacement with a peak value of 3×10^{-7} m. At this point, the solution error of the workpiece-fixture dynamic model is 12.0%, which indicates a relatively high calculation accuracy. Figure 9(b) shows that the workpiece vibration response with a single support is 2.227×10^{-7} m under a 10 kΩ resistance, which represents a 25.8% reduction compared with that without support. The error between theoretical predicted value and the experimental value is 18.2%. =0.182. Figure 9(c) shows that the workpiece vibration response is 2.162×10^{-7} m under a 20 kΩ resistance. This is a 27.9% decrease compared with the unsupported workpiece, and a 2.91% decrease compared with the response under 10 kΩ, and the theoretical prediction error is 16.3%. Figure 9(d) shows that the vibration response is 2.086×10^{-7} m under a 30 kΩ resistance. This corresponds to a 30.5% reduction compared with the unsupported state and a 3.49% reduction compared to the response under 20 kΩ. At this point, the error between the theoretical prediction value and the experiment value is the smallest and at 14.3%. From Figure 9(e), for 40 kΩ, the response is 2.179×10^{-7} m, a 27.4% reduction from the unsupported case but a 4.44% increase compared to 30 kΩ. The prediction error rises to 17.5%. From Figure 9(f), at 50 kΩ, the response is 2.373×10^{-7} m, showing a 20.9% reduction from no support but an 8.9% increase over 40 kΩ. The prediction error is 18.4%. In general, the theoretical predictions align well with experimental results. A single piezoelectric fixture suppresses vibration by 20.9% to 27.4%. The suppression effect first strengthens and then weakens as the external circuit resistance increases. When the resistance R_L is 30 kΩ， the piezoelectric support structure has the appropriate modal frequency, and has the highest energy harvesting efficiency and vibration suppression effect.

Figure 9: Comparison of vibration displacement responses between the workpiece with one piezoelectric support and no support under 200 Hz excitation: (a) without support, (b) 10 kΩ, (c) 20 kΩ, (d) 30 kΩ, (e) 40 kΩ, (f)50 kΩ

Figure 10(a) shows the workpiece vibration displacement without support with a peak value of 3×10^{-7} m, which is the same as that in Figure 9(a).

Figure 10(b) indicates that the workpiece vibration response is 1.713×10^{-7} m under a resistance of 10 kΩ with 2 supports. This represents a 42.9% reduction compared to the workpiece without support, and the error between the theoretical prediction of the workpiece vibration response and the experimental result is 23.1%. From Figure 10(c), at 20 kΩ, the vibration response is 1.691×10^{-7} m, a 43.6% reduction from no support and 1.31% lower than the 10 kΩ condition. The prediction error is 17.32%. From Figure 10(d), at 30 kΩ, the response reaches 1.675×10^{-7} m, achieving the best suppression effect (44.2% reduction from no support and 0.89% improvement over 20 kΩ). The prediction error is minimized at 17.23%. From Figure 10(e), for 40 kΩ, the response is 1.690×10^{-7} m (43.7% reduction from no support but a 0.89% increase compared to 30 kΩ). The prediction error is 16.24%. From Figure 10(f), at 50 kΩ, the response rises to 1.795×10^{-7} m, reflecting a 40.2% reduction from no support but a 6.23% increase over 40 kΩ. The prediction error is 16.4%. In general, theoretical predictions align well with experiments. Two piezoelectric fixtures suppress vibration by 40.2% to 44.2%, following a trend of initial strengthening then weakening as resistance increases. Optimal suppression (44.2%) occurs at 30 kΩ, while the weakest effect (40.2%) appears at 50 kΩ, which matchs theoretical expectations.

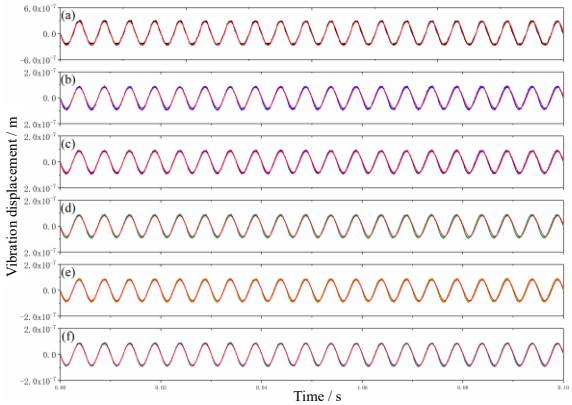

Figure 10: Comparison of vibration displacement responses between the workpiece with two piezoelectric support and no support under 200 Hz excitation: (a) without support, (b) 10 kΩ, (c) 20 kΩ, (d) 30 kΩ, (e) 40 kΩ, (f)50 kΩ

Figure 11 is a comparative diagram illustrating the vibration response of the workpiece without support versus that with 4 supports. Figure 11(a) shows the vibration response of the workpiece without support, which is consistent with that in Figure 10(a). From Figure 11(b), with 10 kΩ resistance and 4 supports, the vibration response is 1.253×10^{-7} m, showing a 58.2% reduction from the unsupported case. The error between theoretical prediction and experimental results is 21.2%. From Figure 11(c), at 20 kΩ, the response is 1.237×10^{-7} m (58.8% reduction from no support and 1.25% lower than 10 kΩ). The prediction error is 20.3%. From Figure 11(d), under 30 kΩ, the response reaches 1.225×10^{-7} m, achieving the optimal suppression (59.2% reduction from no support and 0.97% improvement over 20 kΩ). The prediction error is 22.0%. From Figure 11(e), for 40 kΩ, the response is 1.235×10^{-7} m (58.8% reduction from no support but a 0.92% increase compared to 30 kΩ). The error rises to 21.01%. From Figure 11(f), at 50 kΩ, the response is 1.313×10^{-7} m (56.2% reduction from no support but a 6.20% increase over 40 kΩ). The prediction error is 17.2%. In general, theoretical predictions align well with experiments. Four piezoelectric fixtures suppress vibration by 56.2% to 59.2%. The best suppression (59.2%) occurs at 30 kΩ, while the weakest effect (56.2%) appears at 50 kΩ, consistent with theoretical predictions and meeting the design goals of the vibration energy harvesting structure.

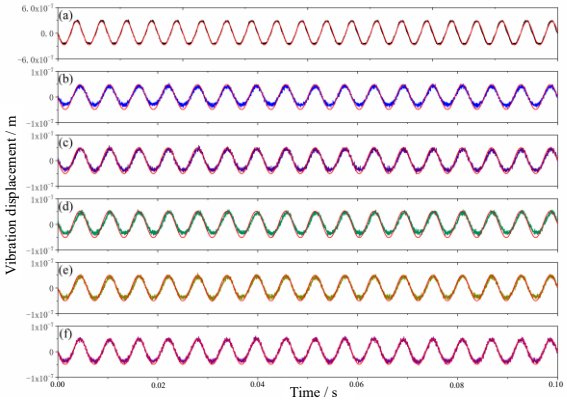

Figure 11: Comparison of vibration displacement responses between the workpiece with four piezoelectric support and no support under 200 Hz excitation: (a) without support, (b) 10 kΩ, (c) 20 kΩ, (d) 30 kΩ, (e) 40 kΩ, (f)50 kΩ

From the above experimental results, it can be observed that the proposed model effectively predicts the system vibration response well. The prediction error without support is larger than that with the supported system, and the theoretical predicted values consistently exceed the measured values. This discrepancy arises because the additional preload introduced during the assembly of the piezoelectric support structures and it increases the equivalent stiffness of the support structure, ultimately leading to the aforementioned discrepancies.

3.2 Workpiece-Fixture System Milling Vibration Control Experiment

To better verify the effective suppression of the workpiece-piezoelectric fixture system, a series of

milling tests were designed, and the milling site is shown in Figure 12. For this purpose, a fixture layout with 4 piezoelectric supports was selected, and machining experiments on the workpiece were conducted using different external circuit resistances. In machining, an 8 mm two-flute end mill was used for the machining of the thin-walled workpiece. The cutting parameters were spindle speed 1500 r/min, axial depth of cut 0.2 mm and feed rate 120 mm/min. A 30 kΩ resistance was adopted and the vibration state of the workpiece was tested using the acceleration sensor fixed on the workpiece and the piezoelectric output voltage. Among the tests, the acceleration sensor signals and the voltage signals of the piezoelectric support structure during machining were collected and analyzed, and the acceleration sensor signal and its frequency spectrum are shown in Figure 13, and the voltage signal generated by the piezoelectric support structure and its frequency spectrum are shown in Figure 14.

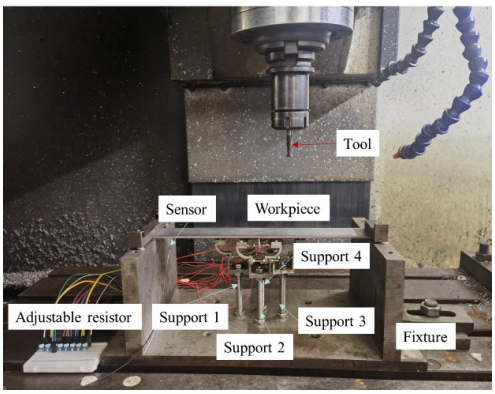

Figure 12: Schematic diagram of the milling device

Figure 13 shows the vibration acceleration signal and its frequency spectrum during machining. As shown in Figure 13(a), the vibration acceleration of the workpiece exhibits periodic peaks with the maximum amplitude collected by the acceleration sensor being 4090.9 m/s^2. From Figure 13(b), it can be observed that the vibration response signal is a continuous harmonic signal, which originates from the excitation frequency caused by the cutter tooth passing frequency and its harmonics. Meanwhile, a peak appears at 0.763 Hz. Figure 14 shows the voltage signal generated by the piezoelectric support component during machining and its frequency spectrum. The externally output voltage of the vibration system fluctuates periodically, and the occurrence trend of each peak is generally similar to that in Figure 13(a), but the proportions corresponding to the peaks are different. At this point, the maximum voltage collected by the piezoelectric fixture is 346.8 mV. From Figure 14(b), it can be seen that the piezoelectric support unit also collects continuous harmonic signals, but its distribution differs significantly from that in Figure 13(b). Moreover, when the frequency range exceeds 300 Hz, the piezoelectric fixture fails to collect signals of many frequencies compared to the signals collected by the acceleration sensor.

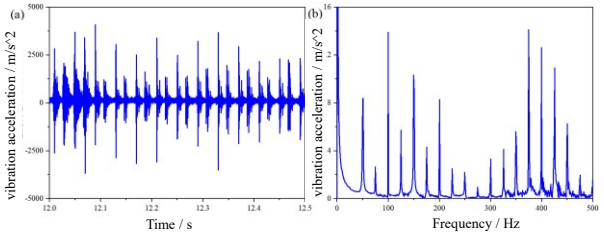

Figure 13: Vibration acceleration signal and its frequency spectrum in milling. (a) Acceleration signal, (b) Frequency spectrum

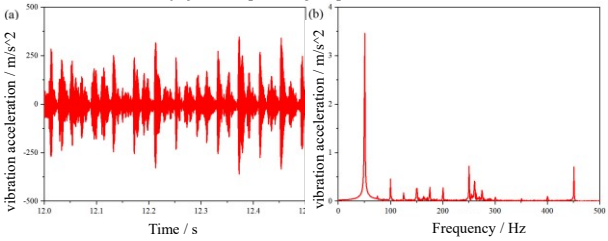

Figure 14: Voltage signal generated by the piezoelectric support component during machining and its frequency spectrum. (a) Voltage signal, (b) Frequency spectrum

Several milling tests were conducted to obtain the workpiece vibration acceleration under different control parameters. Only one group of data was randomly selected for analysis, and the vibration acceleration is shown in Figure 15. According to Figure 15(a), when the vibration control parameter is 10 kΩ with 4 supports, the maximum vibration acceleration of the workpiece is 2975.013 m/s^2, the minimum is 0.006 m/s^2, the mean value is 376.558 m/s^2, and the mean absolute deviation (MAD) is 455.78 m/s^2. Evaluating the vibration based on the MAD shows that the vibration is reduced by 73.33% compared to the unsupported state. From Figure 15(b), it can be obtained that when the control parameter is 20 kΩ, the maximum vibration acceleration is 4685.977 m/s^2, the minimum is 0.008 m/s^2, the mean value is 438.381 m/s^2, and the MAD is 568.761 m/s^2. At this point, the workpiece vibration acceleration is reduced by 66.72% compared to the unsupported state and increased by 24.79% compared to that at 10kΩ, which differs from the trend of the exciter test. As shown from Figure 15(c), when the control parameter is 30kΩ, the maximum vibration acceleration is 1145.851 m/s^2, the minimum is 0.012 m/s^2, the mean value is 149.142 m/s^2, and the MAD is 182.844 m/s^2. Under this condition, the workpiece's vibration acceleration is reduced by 89.30% compared to the unsupported state and by 67.85% compared to that at 20kΩ. Consistent with expectations, the best vibration suppression effect is achieved at this point. As

indicated in Figure 15(d), when the control parameter is 40kΩ, the maximum vibration response of the workpiece-piezoelectric fixture is 5239.749 m/s^2, the minimum is 0.022 m/s^2, the mean value is 711.878 m/s^2, and the MAD is 945.874 m/s^2. Under the current condition, the vibration acceleration is reduced by 44.65% compared to the unsupported state and increased by 417.31% compared to that at 30kΩ, meaning the piezoelectric supports exhibit the worst vibration suppression capability for the workpiece at this point. From Figure 15(e), it can be seen that when the control parameter is 50kΩ, the maximum vibration response of the workpiece is 5239.749 m/s^2, the minimum is 0 m/s^2, the mean value is 616.913 m/s^2, and the MAD is 818.000 m/s^2. At this time, the vibration acceleration is reduced by 52.13% compared to the unsupported state and by 13.52% compared to that at 40kΩ. From Figure 15(f), it can be observed that when 4 piezoelectric support structures are used, the maximum vibration acceleration of the workpiece is 5239.734 m/s^2, the minimum is 0.289 m/s^2, the mean value is 1298.976 m/s^2, and the MAD is 1555.666 m/s^2. This represents an 8.97% reduction in vibration acceleration compared to the unsupported workpiece, and a 64.47% higher vibration acceleration than that with piezoelectric supports at 50 kΩ, indicating that the vibration suppression effect of the piezoelectric support structures is worse than that of the piezoelectric supports. As shown in Figure 15(g), during the machining process, due to the low stiffness of the workpiece, the workpiece exhibits significant vibration: the maximum vibration acceleration reaches 5239.749 m/s^2, the minimum vibration is 0.05 m/s^2, the median is 1393.354 m/s^2, and the MAD is 1708.94 m/s^2.

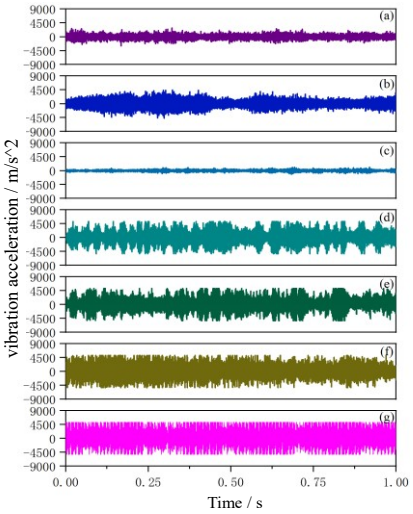

Figure 15: Vibration acceleration of the workpiece during machining under different conditions. (a) 10 kΩ, (b) 20 kΩ, (c) 30 kΩ, (d) 40 kΩ, (e) 50 kΩ, (f) 4 supports, (g) No support

From the above analysis, it can be concluded that the piezoelectric support exhibits a significant vibration suppression effect on the system under different control resistances. Moreover, the most remarkable vibration suppression effect is achieved when the resistance is 30 kΩ, which provides a new solution for the subsequent precision machining of thin-walled parts.

4. Conclusions

Thin-walled blades are characterized by complex shapes, thin walls, and low stiffness. Due to material removal and large cutting forces, the system exhibits pronounced time-varying dynamic characteristics, then, severe vibrations occur in thin-walled parts during machining, which seriously affects their machining quality and efficiency. To address the above issues, a piezoelectric piezoelectric support structures structural units are designed based on on the vibration characteristics of thin-walled workpieces under complex constraints, and used to support the workpiece to suppresses machining vibrations, and a workpiece-fixture dynamic model for thin-walled blade parts is established by the energy method based on piezoelectric vibration energy collection structure, and the machining vibrations are effectively suppressed by employing piezoelectric piezoelectric support structures structural units. The main conclusions obtained in the research process are as follows:

(1) Considering the structure of thin-walled parts and machining processes, an optimized piezoelectric energy-harvesting support structure was designed.

(2) Taking the influence of piezoelectric support structures on the dynamic characteristics of thin-walled parts into account, the layout of support positions for the piezoelectric energy-harvesting support structure in the fixture was simulated and optimized using the finite element software COMSOL, and the fixture configuration was determined.

(3) The influence of the piezoelectric energy-harvesting fixture on the vibration characteristics of the workpiece was analyzed, and a dynamic model of the thin-walled workpiece-fixture system based on the piezoelectric energy-harvesting support structure was established.

(4) To verify the effectiveness of the dynamic model of the workpiece-fixture system, an exciter was used to excite the workpiece-piezoelectric fixture system. Resistance can affect the modal frequency of piezoelectric support structures, thereby influencing the energy absorption efficiency and vibration suppression effect of piezoelectric energy-harvesting fixture. And it was also found that the system achieves the optimal vibration

suppression effect under the control parameter of 30 kΩ when the workpiece is in stable cutting.

Acknowledgement

This work was supported by the Aeronautical Science Foundation of China (2024M044012001).

References

[1] FRAHM H. Device for damping vibrations of bodies: US989958A. 1911-04-18.

[2] J.P. DEN HARTOG. Mechanical Vibrations, 4th ed. Dover Publication, New York, 1985.

[3] Zilletti M, Elliott, S J, Rustighi E. (2012). Optimisation of dynamic vibration absorbers to minimise kinetic energy and maximise internal power dissipation. Journal of sound and vibration, 331(18): 4093-4100. doi: 10.1016/j.jsv.2012.04.023.

[4] Kela L, Vähäoja, P. (2009). Recent Studies of Adaptive Tuned Vibration Absorbers/Neutralizers. Applied mechanics reviews, 62(6): 60801-60809. doi: 10.1115/1.3183639

[5] Brennan M J. (2006). Some Recent Developments in Adaptive Tuned Vibration Absorbers/Neutralisers. Shock and vibration, 13(4-5): 531-543. doi: 10.1155/2006/563934.

[6] Lee C Y, Chen C C, Yang T H, Lin C J. (2012). Structural vibration control using a tunable hybrid shape memory material vibration absorber. Journal of intelligent material systems and structures, 23(15): 1725-1734. doi: 10.1177/1045389X12451190

[7] Zilletti M, Gardonio P, Elliott S J. (2014). Optimisation of a velocity feedback controller to minimise kinetic energy and maximise power dissipation. Journal of sound and vibration, 333(19): 4405-4414. doi: 10.1016/j.jsv.2014.04.036

[8] Vyhlídal T, Olgac N, Kucera V. (2014). Delayed resonator with acceleration feedback-Complete stability analysis by spectral methods and vibration absorber design. Journal of sound and vibration, 333(25): 6781-6795. doi: 10.1016/j.jsv.2014.08.002

[9] Alujevic N, Tomac I, Gardonio P. (2012). Tuneable vibration absorber using acceleration and displacement feedback. Journal of sound and vibration, 331(12): 2713-2728. doi: 10.1016/j.jsv.2012.01.012

[10] Qi R, Wang L, Jin J M, Yuan L S, Zhang D D, Ge Y N. (2023). Enhanced Semi-active piezoelectric vibration control method with shunt circuit by energy dissipations switching. Mechanical Systems and Signal Processing, 201: 110671. DOI: 10.1016/j.ymssp.2023.110671

[11] Ibrahim S W, Ali W G. (2012). A review on frequency tuning methods for piezoelectric energy harvesting systems. 4, 062703. doi: 10.1063/1.4766892

[12] Cellular A C, Monteiro L L D, Savi M A. (2018). Numerical investigation of nonlinear mechanical and constitutive effects on piezoelectric vibration-based energy harvesting. TM-TECHNISCHES MESSEN, 85(9): 565-579. doi: 10.1515/teme-2017-0070

[13] Hadas Z, Vetiska V, Vetiska J, Krejsa J. (2016). Analysis and efficiency measurement of electromagnetic vibration energy harvesting system. Microsystem technologies : sensors, actuators, systems integration, 22(7): 1767-1779. doi: 10.1007/s00542-016-2832-4

[14] Yan B, Yu N, Ma H Y, Wu C Y. (2022). A theory for bistable vibration isolators. Mechanical Systems and Signal Processing, 167: 108507. doi: 10.1016/j.ymssp.2021.108507

[15] Huang D M, Zhou S X, Li R H, Yurchenko D. (2022). On the analysis of the tristable vibration isolation system with delayed feedback control under parametric excitation. Mechanical Systems and Signal Processing, 164: 108207. doi: 10.1016/j.ymssp.2021.108207

[16] Yan B, Yu N, Wang Z H, Wu C A Y, Wang S, Zhang W M. (2022). Lever-type quasi-zero stiffness vibration isolator with magnetic spring. Journal of Sound and Vibration, 527: 116865. doi: 10.1016/j.jsv.2022.116865

[17] Anton S R, Sodano H A. (2007). A review of power harvesting using piezoelectric materials (2003–2006). Smart materials and structures, 16(3): R1-R21. doi: 10.1088/0964-1726/16/3/R01

[18] SHAIKH F K, ZEADALLY S. (2016). Energy harvesting in wireless sensor networks: A comprehensive review. Renewable and Sustainable Energy Reviews, 55: 1041-1054.

[19] Lee S H, Jeong C K, Hwang G T, Lee K J. (2015). Self-powered flexible inorganic electronic system. Nano Energy, 14: 111-125. doi: 10.1016/j.nanoen.2014.12.003

[20] duToit N E, Wardle B L, Kim S G. (2005). Design considerations for MEMS-scale piezoelectric mechanical vibration energy harvesters. Integrated ferroelectrics, 71(1): 121-160. doi: 10.1080/10584580590964574

[21] Adhikari S, Friswell M I, Inman D J. (2009). Piezoelectric energy harvesting from broadband random vibrations. Smart materials and structures, 18(11): 115005. doi: 10.1088/0964-1726/18/11/115005

[22] Wang H Y, Shan X B, Xie T. (2012). An energy harvester combining a piezoelectric cantilever and a single degree of freedom elastic system. Journal of Zhejiang University. A. Science, 13(7): 526-537. doi: 10.1631/jzus.A1100344

[23] Ali S F, Adhikari S. (2013). Energy Harvesting Dynamic Vibration Absorbers. Journal of Applied Mechanics, 2013,80(4). doi: 10.1115/1.4007967

[24] DIPAK S, RAJARATHINAM M, ALI S F. Energy harvesting dynamic vibration absorber under random vibration[C]//: IEEE, 2013: 1241-1246.

[25] Sapinski B. Experimental study of a self-powered and sensing MR-damper-based vibration control system. SMART MATERIALS AND STRUCTURES, 2011,20(10). doi: 10.1088/0964-1726/20/10/105007

[26] Choi K M, Jung H J, Lee H J, Cho S W. (2007). Feasibility study of an MR damper-based smart passive control system employing an electromagnetic induction device. Smart materials and structures, 16(6): 2323-2329. doi: 10.1088/0964-1726/16/6/036

[27] Fang L, Zheng Q W, Hou W C, Zheng L, Li H X. (2022). A self-powered vibration sensor based on the coupling of triboelectric nanogenerator and electromagnetic generator. Nano Energy, 97: 107164. doi: 10.1016/j.nanoen.2022.107164

[28] Chatziathanasiou G M, Chrysochoidis N A, Saravanos D A. (2022). A semi-active shunted piezoelectric tuned mass damper for robust vibration control. Journal of Vibration and Control, 28(21-22): 2969-2983. doi: 10.1177/10775463211026487

[29] Manzoni S, Berardengo M, Boccuto F, Vanali M. (2023). Piezoelectric-shunt-based approach for multi-mode adaptive tuned mass dampers. Mechanical Systems and Signal Processing, 200: 110537. doi: 10.1016/j.ymssp.2023.110537